COMPARISON BETWEEN ACTUAL AND EQUIVALENT CRACK RESISTANCE R-CURVES FOR TIMBER AND TIMBER BOND UNDER MODE-II FRACTURE

Shaikh Atikur Rahman[1], Mahmud Ashraf[2] Mahbube Subhani[3]

ABSTRACT: This paper focuses on Mode-II fracture behaviour of solid timber and timber adhesive bond using end notched flexure (ENF) test. Mode-II strain energy release rates are obtained using three different data reduction methods known as compliance calibration (CC), direct beam theory (DBT) and corrected beam theory (CBT) that require actual crack length monitoring. At the same time, the compliance-based beam method (CBBM) is evaluated without the need for actual crack length measurements by considering an equivalent crack length. In both cases, the Mode-II strain energy release rates (G_{II}) obtained for the timber adhesive bond interface was found to be approximately 20% higher compared to timber fracture. The strain energy release rates calculated from actual crack and equivalent crack length values show similar trends in resistance curves. However, initial strain energy release rate (G_{II0}) and critical strain energy rate (G_{IIC}) for Mode-II significantly varies in actual crack methods than the equivalent crack method.

1 INTRODUCTION

Currently, all design guidelines for timber and engineered timber products (ETPs) are based on the maximum elastic stress and stiffness criteria for strength analysis. However, it fails to attain the material's post-elastic plastic behaviour and localised failure owing to defects like cracks or delamination [1]. In the stress/stiffness method, the structural component is considered as a continuous homogenous material, which is not relevant to naturally grown materials such as timber. Those defects are often considered using a strength reduction factor in a conventional stress/stiffness design technique, which is very conservative for real-life structure.

To overcome such limitations, fracture mechanics-based design approach in timber structure could be a rational alternative. Fracture mechanics is often utilised in material testing on samples with well-defined characteristics [2]. It is, however, rarely employed in engineering design with structural elements of arbitrary shape. Fracture characterisation of softwood timber is essential, especially for the design of various timber joints, notches, holes, and connections. Timber failure can cause catastrophe as they lead to highly brittle failure produced by tension and shear acting perpendicular to grain direction of timber [1, 3, 4].

Material fracture characterisation is therefore vital in giving accurate fracture characteristics such as the critical strain energy release rate, $G_{I/IIc}$, which is defined as the material's resistance to crack propagation. Furthermore, using experimental $G_{I/IIc}$, the current design approach for brittle splitting failure prediction of connections loaded perpendicular to the grain (critical failure mode in timber structures) defined in Eurocode 5 (EC5). A new fracture based design approach is currently used in a few design standards only for certain connection designs [3]. To ensure safe and effective application of timber and ETPs, a comprehensive fracture-based design approach is necessary. Comprehensive knowledge of the fracture properties of solid timber and timber adhesive bond is a prerequisite to develop fracture-based design approach. Fracture behaviour of timber has recently gained momentum and fracture mechanics based numerical models has been shown to provide a superior mechanical rupture description than traditional strength-based techniques. The ability to consider the material non-linearity beyond the fracture tip, the limited stress capacity, and the material's non-linear stress-deformation performance at the crack tip can be address by non-liner fracture mechanics (NLFM) [3]. This may be accomplished by a variety of methods, the most straightforward of which is to characterise the material's fracture behaviour using

[1] Shaikh Atikur Rahman, Deakin University, Australia, sarahman@deakin.edu.au
[2]Mahmud Ashraf, Deakin University, Australia, mahmud.ashraf@deakin.edu.au

[3]Mahbube Subhani, Deakin University, Australia, mahbube.subhani@deakin.edu.au

crack resistance R-curve or stress deformation relation that incorporates material softening, generally referred to as σ-w curve. Continuum damage mechanics (CDM) or cohesive zone (CZM) based material modelling in finite element (FE) simulation have been shown to capture fracture behaviour of timber [5].

Two methods are typically used to identify the material fracture resistance, i.e., the stress intensity factor approach and the strain energy-based approach. The energy-based technique is used in this study since it is more suited to orthotropic materials like timber, and the derivation of the main equation is less dependent on sample geometry [3]. Timber is strong if load is applied in parallel to grain direction while very weak against perpendicular to grain loading. Timber parallel longitudinal fibre is strong and acts like reinforcement against any displacement. Thus, Parallel loading to the grain direction normally involves with longitudinal fibre breaking in LR and LT fracture plane which has significantly higher crack resistance than any other plane of timber. On the other hand, fibre has lots of gaps, faults and has less crack resistance while crack propagating along longitudinal direction in RL and TL plane. Therefore, crack plane RL and TL is one of the weakest crack planes of timber and widely seen in end notch, circular, rectangular holes and various timber connections [6]. Additionally, adhesives are used in most of the engineered timber products (ETPs) and timber connections. Failure of timber adhesive bond can be highly brittle and catastrophic like timber fracture due to perpendicular loading. Due to the softness of timber material, timber bond delamination shows combination of bond fracture and timber splitting along the longitudinal direction. Therefore, it is important to identify pure bond delamination resistance and timber resistance along the bond interface, which is usually the longitudinal direction of timber.

This paper presents Mode-II fracture behaviour of timber and timber adhesive bond using end notched flexure (ENF) test. In the last decades, methods to evaluate fracture energies (strain energy release rates in Mode-II (G_{II})) have been developed using simple analytical methods as well as complex compliance-based beam methods (CBBM) [1]. Crack resistance curves, commonly known as R-curves, are generated from the evolution of fracture energy release rate in relation to the crack length. Due to the complexities of monitoring actual crack length, an equivalent crack method is widely used for different modes of fracture tests. It is worth noting that fracture theories were mostly developed for fibre reinforced composites and there are significant gaps in their application for natural bio composite materials such as timber and ETP. Lack of specific guidelines and standards on timber fracture tests, R-curves generated only from the load-displacement behaviour may sometime lead to wrong projection of strain energy release rate due to inconsistent specimen size and testing procedure. Equivalent crack method has advantage for ENF test, but it also requires proper validation from actual crack length monitoring during

test. Using digital image corelation (DIC) system in crack detection and crack length measurement will remove complexities of traditional crack identification techniques and increase the accuracy and robustness of actual crack method. This study presents a detailed comparison between actual and equivalent crack resistance R-curves to highlight the potential as well as the challenges associated with the equivalent crack method. This study also compare the Mode-II fracture behaviour of solid timber and timber adhesive bond.

2   MATERIALS AND METHODS

Samples required for ENF testing were produced from the Australian softwood timber species Radiata pine. The prepared timber specimens were maintained in a chamber at 20°C and 65% relative humidity until the moisture content reached equilibrium. Before the test, the density of each specimen was tested, and the average density was determined to be 580(±44) kg/m3. The average moisture content for all samples was 10.8(±0.94) percent. Figure 1 depicts a schematic of an ENF sample for solid timber. ENF timber samples have cross-sections of 20 mm×20 mm, and 500 mm long. The span length was kept at 460 mm to ensure smooth and steady fracture propagation, as previously reported by De Moura, et al. [7]. Carlsson, et al. [8] proposed that the initial fracture length (a_0) should be more than 0.7L to enable steady crack propagation. The first crack length (a_0) was taken as 162 mm long, greater than 0.7L, where L is half the specimen span length (= 230 mm). It is difficult to maintain smooth straight initial crack line using handheld saw blade and table saw machine does not have blades thinner than 0.80 mm. Therefore, to keep the initial notch width as small as feasible, a 162 mm notch was cut using a 0.80 mm blade of a table saw machine. The following notch was then cut using a handheld saw blade, and the width of the last 20 mm notch was kept 0.50 mm. Timber adhesive bond samples were made by bonding two different timber boards with 20 mm width and 10 mm height to ensure the same cross section (20 mm×20 mm) as solid timber samples. Glue specifications were used to maintain the bond curing time, moisture content, and relative humidity.
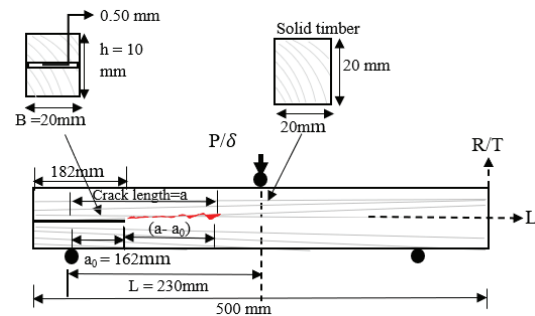
Figure 1: Geometric dimensions and set-up of ENF solid timber specimen.

Polyurethane based adhesive HB S309 PURBOND was used for timber adhesive bond. A schematic overview

and test set-up of the ENF test is shown in Figure 2. The timber adhesive bond specimen has same dimension as solid timber of 500 (l) × 20 (b) ×20 (t) mm. A thin plastic tape with a thickness of 0.1 mm was placed between two timber beam joints along 182 mm length to make an initial notch. This thin plastic produced a 0.1 mm gap at the initial notch, and remaining length of the sample were bonded properly. This method was implemented to protect timber fibres from damaging due to mechanical cutting.
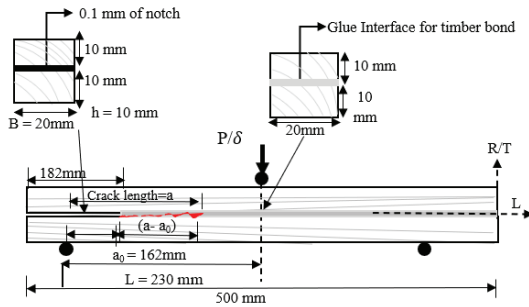
Figure 2: *Schematic overview and set-up of ENF timber adhesive bond test*

The test was conducted using a 10 KN Instron load frame with a displacement control of 5 mm/min. All the test was captured by the digital image corelation (DIC) to identify the crack and monitor the crack propagation length. DIC was calibrated and verified prior to test commencement with known displacement from Instron load frame. The Instron load frame and DIC system were ensured to have the same frequency so that both data can merge. The displacement (δ) was measured at the load application point and a continuous crack growth length (a) was measured by DIC. The testing set-up was identical in timber and timber bond fracture tests.

2.1 DATA REDUCTION METHODS

A bending load (p) is applied at the mid span for ENF test, causing Mode-II fracture propagation over the length of the test ($L-a_0$). Instron load frame was used to determine the applied load (p) and displacement (δ) at the loading point while continuous crack propagation length ($a-a_0$) is obtained by DIC. The basic formula to calculate strain energy release rate was introduce by Irwin-Kies [2]. The formula is based on compliance C, which is determined from load and displacement, as shown in Eq. (1)

$$G_{II} = \frac{P^2}{2B}\frac{dC}{da} \qquad (1)$$

Several data reduction schemes exist to calculate the evolution of Mode-II strain energy release rates [9]. Mode-II data reduction techniques are classified into two types: actual crack identification methods and equivalent crack methods. ASTM-D7905 [10] (Standard test method for fibre-reinforced polymer) suggested to use compliance calibration (CC), direct beam theory (DBT) and corrected beam theory (CBT) method based on actual crack monitoring. The accuracy and robustness of those methods largely depend on precision in monitoring

actual crack length. Several investigations were carried out in the absence of a rigors technique for measuring crack length, resulting in a broad range of timber fracture energy[8, 11]. With the help of DIC system crack identification and monitoring can be more appealing than conventional methods. According to the compliance calibration (CC) method, strain energy release rate is determined using Eq (2).

$$G_{IIc} = \frac{3ma^2P^2}{2B} \qquad (2)$$

where m is the coefficient of CC obtained from the slope of compliance (C) verses crack length cube (a^3); B is the specimen width. Therefore, CC is not only dependent on load and crack length but also rely on experimental calibration by compliance. A simplified beam theory known as direct beam theory (DBT) evaluates Mode-II fracture energy directly from load, displacement and other constant geometric values. However, DBT does not implement any experimental data reduction scheme. The load head displacement from ENF test is comparatively higher than other testing method like compact shear test (CS) and tapered end notched flexure TENF [7]. Due to those issues DBT may overestimate the fracture energy than other method. DBT is also based on actual crack monitoring. DBT method can be expressed as shown in Eq (3):

$$G_{IIc} = \frac{9a^2P\delta}{2B(2L^3 + 3a^3)} \qquad (3)$$

To address the limitation of DBT, a correction factor of introducing flexural modulus is added to the fracture energy calculation. This corrected method is known as corrected beam theory (CBT) also a classical method based on actual crack monitoring [9]. In CBT, G_{IIC} is determined from Eq 4.

$$G_{IIc} = \frac{9a^2P^2}{2B^2h^3E_f} \qquad (4)$$

where E_f is calculated using Eq (5) and initial compliance (C_0) determined from the ratio of displacement and load.

$$E_f = \frac{L^3}{4Bh^3C_0} \qquad (5)$$

All aforementioned methods (CC, DBT, CBT) depend on accurate measurement of the actual crack length during test. The compliance-based beam method (CBBM) [12], which is based on Timoshenko beam theory, can predict G_{II} using the load-displacement data [9] without actual crack measurements. CBBM determines G_{II} following Eq (6) to (10).

$$G_{IIc} = \frac{9P^2a_{eq}^2}{16B^2h^3E_f} \qquad (6)$$

$$C = \frac{3a^3 + 2L^3}{8Bh^3E_{f(CBBM)}} + \frac{3L}{10BhG_{LR}} \qquad (7)$$

where $E_{f(CBBM)}$ is the flexural modulus; $I = 8Bh3/12$ is the second moment of area and G_{LR} is the shear modulus in longitudinal-radial plane. Initial elastic compliance C_0 and initial crack length a_0 are used to calculate corrected

flexure modulus $E_{f(CBBM)}$ using Equation (8)

$$E_{f(CBBM)} = \frac{3a_0^3 + 2L^3}{12I}\left(C_0 - \frac{3L}{5G_{LR}A}\right)^{-1} \quad (8)$$

To get an equivalent crack length at each point, the experimental compliance C should be replaced by a corrected compliance C_C. An equivalent crack length a_{eq} and the corrected compliance C_C can be determined using Equation (9):

$$a_{eq} = \left[\frac{C_C}{C_{0C}}a_0^3 + \frac{2}{3}\left(\frac{C_C}{C_{0C}} - 1\right)L^3\right]^{1/3} \quad (9)$$

Where $C_C = C - \frac{3L}{5AG_{LR}}$ and $C_{0C} = C_0 - \frac{3L}{5AG_{LR}}$

Once a_{eq} is determined, equation (9) can be modified as G_{II} using Equation (10)

$$G_{II} = \frac{9P^2}{16B^2h^3E_f}\left[\frac{C_C}{C_{0C}}a_0^3 + \frac{2}{3}\left(\frac{C_C}{C_{0C}} - 1\right)L^3\right]^{2/3} \quad (10)$$

CBBM also depends on of the shear modulus in the longitudinal-radial plane G_{LR} but its effect in G_{II} calculation has been reported to be insignificant [13].

3   RESULTS AND DISCUSSION

Figures 3 and 4 illustrate the load versus displacement curves of ENF Mode-II fracture tests on solid timber and timber adhesive bond. The elastic part of the load-displacement curve is linear and has a constant initial slope prior to development of fracture. However, immediately after fracture initiation, the load curve drops to a lower magnitude for both solid timber and timber adhesive bond.
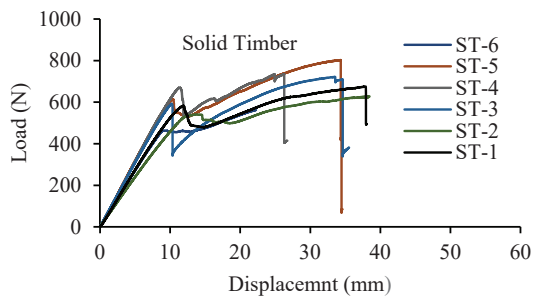
Figure 3: Load vs Displacement from ENF test on sawn timber
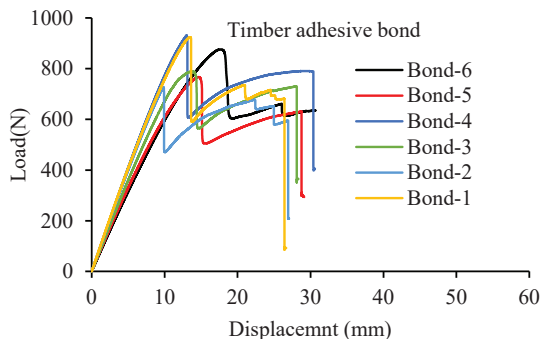
Figure 4: Load vs Displacement from ENF on timber adhesive bond

The post-elastic component of the load-displacement response was highly non-linear and showed variations between samples. Most critically, the post elastic section of the load-displacement curve did not follow linear elastic fracture mechanics (LEFM). To address the Mode-II fracture behaviour of solid timber and timber adhesive bond, advanced nonlinear fracture mechanics-based FEM analysis techniques such as cohesive zone model (CZM) or continuum damaged mechanics (CDM) would be required. It is also obvious from the load-displacement response that, after crack initiation, the timber and timber adhesive bond displayed strain hardening response, which finally led to ductile failure showing better structural response when compared with Mode-I fractures observed in timber [14]. The in-plane shear fracture in RL and TL plane showed slightly ductile failure than tensile fracture. In contrast to solid timber, timber adhesive bond fracture demonstrated higher stiffness and strength.

Crack propagation due to Mode-II loading is typically known as in-plane shear crack. Pure Mode-II shear crack developed due to horizontal movement of two cracked surfaces is characterised by a very thin crack line, which is extremely difficult to visualise using naked eye. The current study, hence, used DIC to identify and monitor exact crack length. Mode-II ENF sample of both solid timber and timber-adhesive bond developed ultra-thin cracks as shown in Figure 5. It is worth noting that unlike Mode-I fracture due to direct tension, the timber and timber adhesive fracture process and crack growth in Mode II was more gradual and consistent.
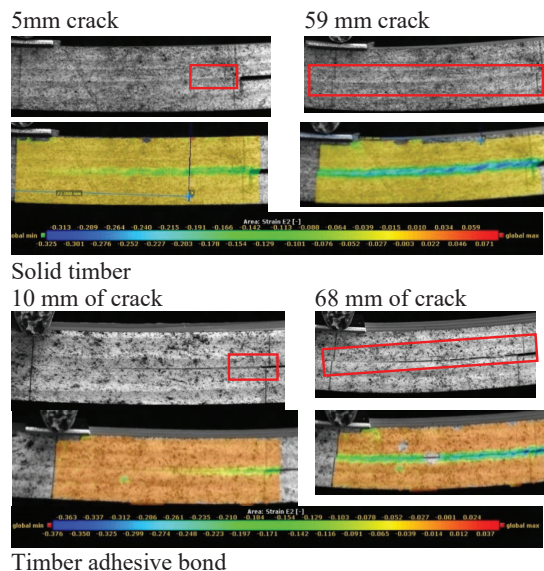
Figure 5: Illustration of crack development in solid timber and timber adhesive bond

3.1   CRACK RESISTANCE R-CURVE

The development of the strain energy release rate (G_{II}) as a function of the crack length is commonly known as R-curve. The area immediately around the crack tip, where

different toughening and softening processes due to many microcracks, cracks-branching, and fibre-bridging, occur, is known as the fracture process zone (FPZ). These non-linear events should be included in R-curve as they have obvious impact on how crack propagates through timber and timber adhesive bond. Since the critical fracture energy (G_c) is determined by the plateau value of these curves, the R-curve is a valuable tool for quantifying the critical fracture energy in the effect of the FPZ. Shape and pattern of R-curve depends on the material's crack resisatnce property. Material crack resistance can have three different shapes as rising R-curve, flat R-curve and falling R-curve [11]. For example Mode-I crack resistance R-curve for timber in RL plane show falling R-curve [14]. A simplified scematic of those three type of R-curves are illustrated in Figure 6. The shape and pattern of R-curve is a important material behaviour to catagorise the type of structural failure due to fracture. The material having falling R-curve (where fracture energy gradually or suddenly decrease with the increase of crack length) causes more catstropic and brittle failure of the structure. With a rising R cuve, material's crack resistance increases after the crack initiation or propagation to a point when G_c is greater than G_0. The specific plane of a maerial with rising R-curve will offer more ductile fracture behaviour than the plane with a falling R-curve.
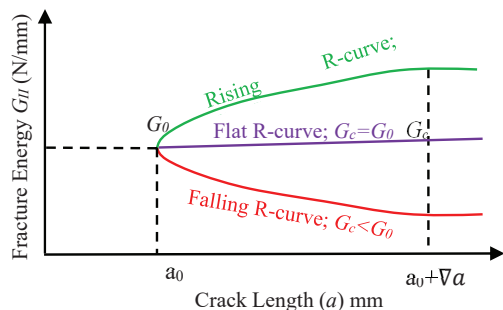
Figure 6: Schematic of different R- curve patterns

To develop crack resistance R-curve for solid timber and timber adhesive bond, all data reduction methods including actual crack method and equivalent crack method were applied. A typical comparison among all data reduction methods for solid timber and timber adhesive bond are shown in Figure 7 and Figure 8. The shape of the R-curve for both solid timber and timber adhesive bond are rising, i.e. crack resistance increase as the crack length propagates showing ductile failure. The governing equation of fracture energy (G_{II}) clearly depends on load, displacement, and corresponding crack length, and hence, hardening or softening responses of load-displacement curve are directly reflected in the corresponding R-curve.
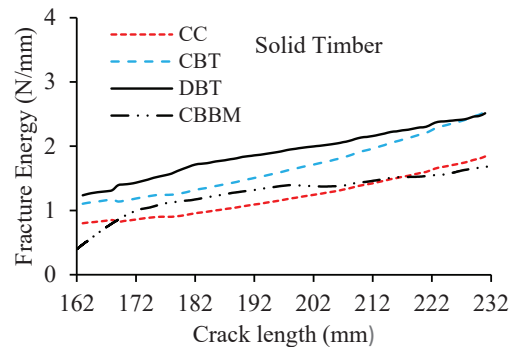
Figure 7: R-curve for solid timber
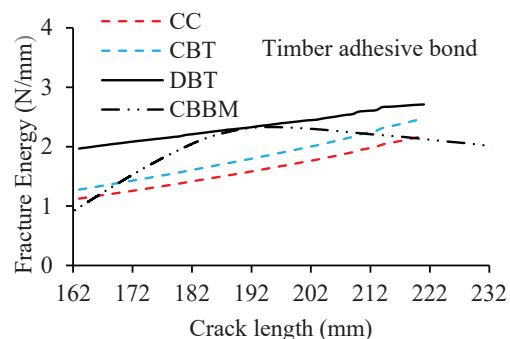
Figure 8: R-curve for timber adhesive bond

3.2 COMPARISON BETWEEN ACTUAL AND EQUIVALENT R-CURVE

R-curves were developed following actual crack methods as CC, CBT and DBT, and all three methods showed similar trends as shown in Figure 7 and Figure 8. However, DBT overestimate the fracture energy than other methods. DBT was simplified beam theory directly formed from load and load head displacement. It is also important to note that DBT does not implement any data reduction scheme which cause wrong prediction of fracture energy. Compliance calibration (CC) and corrected beam theory (CBT) showed well prediction of Mode-II fracture energy, although CBT prediction is higher than CC. In contrast, the fracture energy at crack initiation from CBBM is much lower than those obtained from CC, DBT and CBT. This raises a fundamental issue of identifying crack initiation point for the equivalent crack method. It is worth noting that in Figure 8, the actual crack length from (CC, DBT and CBT) culminated at 222 mm, but the equivalent crack from CBBM goes to the full length of 232 mm as the equivalent crack method cannot differentiate whether the crack was developed due to fracture or specimen damaged due to other material issues such as natural defects, and faulty notch width. In equivalent crack method, fracture energy release rate (G_{II}) is only calculated from load and displacement values, and hence validation with actual crack length measurement is essential. Despite some limitations and shortcomings,

157

CBBM remarkably produced consistent and stable R-curve after the crack initiation. CBBM produced excellent plateau shape in R-curve which signifies the stable energy release rate, known as critical strain energy release rate. The advantages of using CBBM are obvious as the technique does not require any sophisticated equipment such as travelling microscope and DIC system. The critical fracture energy determined using CBBM technique may be used in advanced structural analysis once the fundamental behaviour of the material is validated against classical techniques, i.e., CC/CBT. A comparison of G_{II} obtained from three different data reduction methods for solid timber and timber adhesive bond are summarised in Table 1 and Table 2. Considering the results obtained from six identical solid timber samples, the average fracture energy (G_{II}) from CC, CBT and CBBM are 1.32 N/mm, 1.41 N/mm, and 1.20 N/mm respectively. CBT produce 6.81% higher fracture energy than CC and 17.5% higher than CBBM.

Table 1: *ENF test result on Solid timber (ST)*

Test	Max Load (*N*)	Actual crack monitoring		Equivalent crack method
		CC (*N/mm*) (G_{IIc})	CBT (*N/mm*) (G_{IIc})	CBBM (*N/mm*) (G_{IIc})
ST-1	594.90	1.26	1.34	1.28
ST-2	539.84	1.21	1.30	1.32
ST-3	588.23	1.24	1.34	1.20
ST-4	528.62	1.18	1.27	1.04
ST-5	669.31	1.54	1.63	1.27
ST-6	608.90	1.50	1.59	1.07
Mean	**588.3**	**1.32**	**1.41**	**1.20**
COV%	8	11	11	9

The average Mode-II fracture energy for timber adhesive bond using CC, CBT and CBBM are 1.56N/mm, 1.69N/mm and 1.72N/mm individually. For timber adhesive bond equivalent crack method (CBBM) produced higher fracture energy than CC and CBT. During the crack development process, timber-adhesive bonded specimens experienced higher load than those for solid timber samples (as shown in Figure 3 and Figure 4) resulting in higher compliance (C_0 and C), which eventually contribute to flexural modulus (E_f) and fracture energy (G_{II}) (see the Eq(7-(10).

Table 2: *ENF test results on Timber adhesive bond*

Test	Max Load (*N*)	Actual crack monitoring		Equivalent crack method
		CC (*N/mm*) (G_{IIc})	CBT (*N/mm*) (G_{IIc})	CBBM (*N/mm*) (G_{IIc})
Bond-1	922.01	1.50	1.54	1.83
Bond-2	719.62	1.50	1.69	1.05
Bond-3	787.82	1.68	1.79	1.80
Bond-4	926.34	1.91	2.00	2.00
Bond-5	762.09	1.26	1.38	1.56
Bond-6	875.21	1.56	1.79	2.12
Mean	**832.1**	**1.56**	**1.69**	**1.72**
CV%	10	13	12	22

3.3 COMPARISON BETWEEN SOLID TIMBER AND TIMBER ADHESIVE BOND CRACK RESISTANCE

Results shown in Table 1 and Table 2 indicates that timber-adhesive bond would require more energy to fracture when compared to an equivalent sawn timber. With the same testing configurations, average crack initiation load was almost 42% high in timber bond than that for solid timber, and fracture energy from CC method was 18% high in timber bond than solid timber. An overall response of R-curve for all timber and timber-adhesive bond specimens obtained from CC (as a representative classical method) and CBBM are shown in Figure 9-Figure 12. Crack resistance R-curves for solid timber and timber adhesive bond followed rising R-curve. However, CBBM method for timber adhesive bond showed slightly flat curve after a significant length of crack propagation.
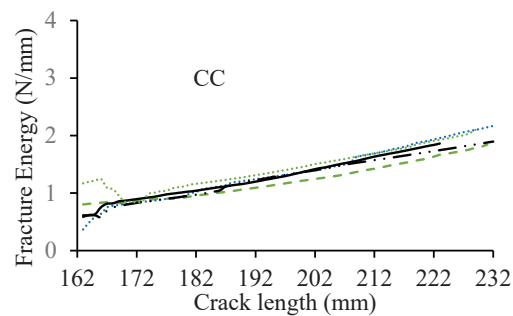
Figure 9: *R-curve for Solid timber using CC.*
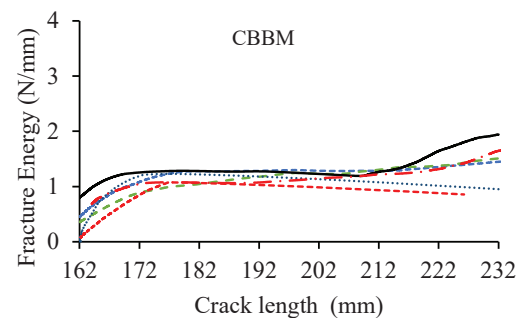
Figure 10: *R-curve for Solid timber using CBBM.*
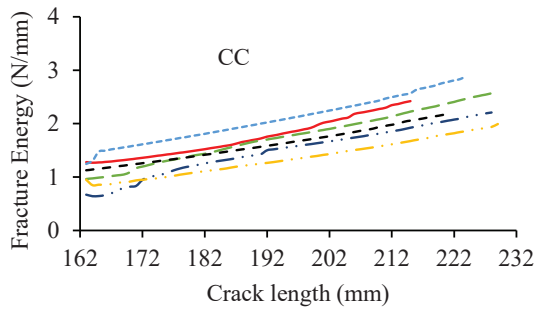
Figure 11: R-curve for timber adhesive bond using CC.
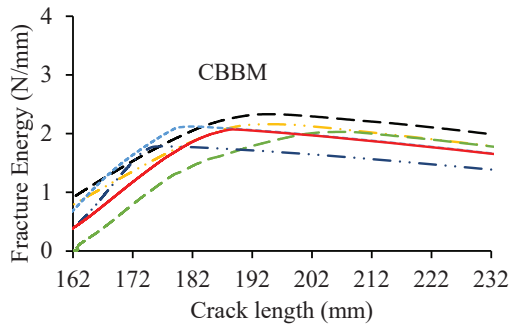
Figure 12: R-curve for timber adhesive bond using CBBM.

4 DISCUSSION

This paper put emphasis on quantifying crack resistance of solid timber and timber adhesive bond under Mode-II fracture using two different techniques, i.e., actual crack method and equivalent crack method. A comparison shown in Table 3 were conducted between Mode-I and Mode-II fracture energy values for various timber species (results in bold are taken from the current study). Mode-II fracture energy for radiata pine was found to be 1.32 N/mm, which is consistent with other Mode II energy levels published in the literature.

Mode-I fracture energy values [5, 12-14] for radiata pine and other species are also shown in Table 3, which shows that Mode-II fracture energy of radiata pine is almost three time higher than its Mode-I fracture energy. This implies that that in case of mixed mode loading, timber structure will be vulnerable to Mode-I cracking. However, in cases where in-plane shear is dominant such as various holes in timber beams for service lines and in various joints, Mode II failure will trigger eventually splitting failure. Since that Mode II fracture in timber and timber adhesive bonding is more ductile than Mode I failure, a combined failure would be structurally preferable to the more catastrophic Mode I failure alone. A typical comparison between Mode-I and Mode-II R-curves is shown in Figure 13, in which R-curve for Mode-I is taken from [14]. Figure 13 clearly demonstrates the distinct difference in R-curves between Mode II and Mode I, with the former gradually rising in

contrast to the latter showing a plateau as crack propagates.

This comparison reiterates the fact that Mode II timber failure shows resistance to cracking and is more ductile than Mode I failure. Additionally, timber fracture energy is compared with those of carbon fiber/epoxy composite laminates in Table 3. It is interesting to see that despite being a natural fibre, timber's resistance to fracture in Mode II is only 35% less than that of carbon fiber/epoxy composite [15].

Table 3: Comparison of energy with different material and different timber species

Mode-I Fracture		Mode-II Fracture	
Species	G_{Ic} (N/mm)	Species	G_{IIc}(N/mm)
Radiata pine[14]	0.48	**Radiata pine**	**1.20-1.41**
Timber adhesive bond[16]	0.48	**Timber adhesive bond**	**1.56-1.72**
spruce[6]	0.30	Eucalyptus globulus[17]	1.54
European beech[6]	0.46	Radiata pine[18]	1.27
CF/EP composite[15]	0.68	CF/EP composite [15]	1.92

This study also examined the difference in fracture behaviour between timber fracture and glue delamination. A thin plastic tape with 0.1 mm thickness was used in ENF bond samples which produced pure bond delamination along the glue line. Although solid timber and timber adhesive bond indicated similar behaviour, timber adhesive bond showed higher stiffness, strength but was less ductile and less stable than solid timber; this clearly highlights the importance of recognition of glue lamination in engineered timber structures.
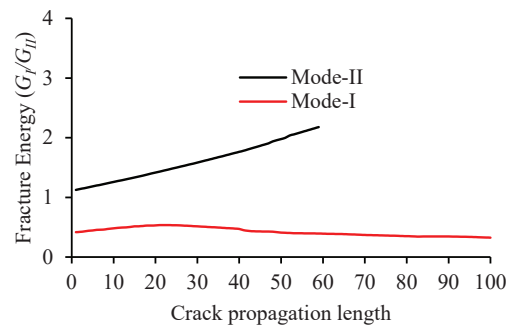
Figure 13: R-curves of timber in Mode-I and Mode-II

In practice, however, glue delamination in softwood timber-adhesive joints is often ignored in both numerical and theoretical analysis of timber structures. Ignoring the glue delamination behaviour in engineered timber products may result in an incorrect prediction of resistance. Fracture properties presented in the current study should be useful in developing reliable numerical models for timber and ETPs such as cross-laminated timber (CLT), glue laminated timber (GLT), glulam etc.

5 CONCLUSION

The current research presents Mode II fracture behaviour of solid timber and timber adhesive bond utilising different data reduction strategies that are based on actual as well as equivalent crack length. In terms of Mode-II crack resistance R-curves, there were notable variations between the real crack method and the equivalent crack method.

Compliance calibration (CC) and corrected beam theory (CBT) methods produced reliable results for Mode-II fracture energy. While DBT fails to offer superior outcomes on Mode-II fracture energy. The equivalent crack method CBBM method showed outstanding response of crack resistance R-curve after crack initiation. However, CBBM suffered to identify the reliable fracture energy at crack initiation point.

A realistic comparison of Mode-II fracture properties between timber and timber adhesive bond were executed. Comparison result shows timber adhesive bond require greater fracture energy to initiate crack in bond line than solid timber. A new technique of creating initial notch without cutting or damaging timber fibre were introduce which produce pure glue delamination and guaranteed stable crack propagation across the glue line.

Digital image correlation (DIC) has been utilised effectively in timber fracture identification and crack length monitoring. Outputs from DIC could be important for cohesive zone modelling and continuum damaged based material modelling to evaluate timber and timber adhesive bond fracture. Finite element models, in conjunction with experimental findings, will give a strong solution for a wide range of difficult circumstances in wood joints and connections.

REFERENCES

[1]   M. Yurrita and J. M. Cabrero, "On the need of distinguishing ductile and brittle failure modes in timber connections with dowel-type fasteners," *Engineering Structures,* vol. 242, p. 112496, 2021/09/01/ 2021, doi: https://doi.org/10.1016/j.engstruct.2021.112496.

[2]   M. F. Kanninen, C. H. Popelar, and A. J. McEvily, "Advanced Fracture Mechanics," *Journal of Engineering Materials and Technology,* vol. 108, no. 2, pp. 199-199, 1986, doi: 10.1115/1.3225862.

[3]   P. Zarnani and P. Quenneville, "Strength of timber connections under potential failure modes: An improved design procedure," *Construction and Building Materials,* vol. 60, pp. 81-90, 2014/06/16/ 2014, doi: https://doi.org/10.1016/j.conbuildmat.2014.02.049.

[4]   N. Dourado, F. G. A. Silva, and M. F. S. F. de Moura, "Fracture behavior of wood-steel dowel joints under quasi-static loading," *Construction and Building Materials,* vol. 176, pp. 14-23, 2018/07/10/ 2018, doi: https://doi.org/10.1016/j.conbuildmat.2018.04.230.

[5]   S. A. Rahman, M. Ashraf, M. Subhani, and J. Reiner, "Comparison of continuum damage models for nonlinear finite element analysis of timber under tension in parallel and perpendicular to grain directions," *European Journal of Wood and Wood Products,* vol. 80, no. 4, pp. 771-790, 2022/08/01 2022, doi: 10.1007/s00107-022-01820-8.

[6]   N. Dourado, M. de Moura, S. Morel, and J. Morais, "Wood fracture characterization under mode I loading using the three-point-bending test. Experimental investigation of Picea abies L," *International Journal of Fracture,* vol. 194, no. 1, pp. 1-9, 2015, doi: https://doi.org/10.1007/s10704-015-0029-y.

[7]   M. F. S. F. De Moura, M. A. L. Silva, A. B. de Morais, and J. J. L. Morais, "Equivalent crack based mode II fracture characterization of wood," *Engineering Fracture Mechanics,* vol. 73, no. 8, pp. 978-993, 2006/05/01/ 2006, doi: https://doi.org/10.1016/j.engfracmech.2006.01.004.

[8]   L. A. Carlsson, J. W. Gillespie, and R. B. Pipes, "On the Analysis and Design of the End Notched Flexure (ENF) Specimen for Mode II Testing," *Journal of Composite Materials,* vol. 20, no. 6, pp. 594-604, 1986/11/01 1986, doi: 10.1177/002199838602000606.

[9]   A. Gliszczynski and N. Wiącek, "Experimental and numerical benchmark study of mode II interlaminar fracture toughness of unidirectional GFRP laminates under shear loading using the end-notched flexure (ENF) test," *Composite Structures,* vol. 258, p. 113190, 2021/02/15/ 2021, doi: https://doi.org/10.1016/j.compstruct.2020.113190.

[10]   ASTM, " D7905/D7905M–19e1," *Standard Test Method for Determination of the Mode II Interlaminar Fracture Toughness of Unidirectional Fiber-Reinforced Polymer Matrix Composites,* p. 20, 2019.

[11]   J. Tiu, R. Belli, and U. Lohbauer, "Rising R-curves in particulate/fiber-reinforced resin composite layered systems," *Journal of the Mechanical Behavior of Biomedical Materials,* vol. 103, p. 103537, 2020/03/01/ 2020, doi: https://doi.org/10.1016/j.jmbbm.2019.103537.

[12]   M. De Moura and A. De Morais, "Equivalent crack based analyses of ENF and ELS tests," *Engineering Fracture Mechanics,* vol. 75, no. 9, pp. 2584-2596, 2008.

[13]   M. F. S. F. d. Moura, M. A. L. Silva, J. J. L. Morais, A. B. d. Morais, and J. J. L. Lousada, "Data reduction scheme for measuring GIIc of wood in end-notched flexure (ENF) tests," vol. 63, no. 1, pp. 99-106, 2009, doi: doi:10.1515/HF.2009.022.

[14]   S. Rahman, M. Ashraf, M. Subhani, and J. Reiner, "Influence of initial crack width in Mode I fracture tests on timber and adhesive timber bonds," in *Current Perspectives and New Directions in Mechanics, Modelling and Design of Structural Systems*: CRC Press, 2022, pp. 1675-1680.

[15]   C. Cheng *et al.*, "Simultaneously improving mode I and mode II fracture toughness of the carbon fiber/epoxy composite laminates via interleaved with uniformly aligned PES fiber webs," *Composites Part A: Applied Science and Manufacturing,* vol. 129, p. 105696, 2020/02/01/ 2020, doi: https://doi.org/10.1016/j.compositesa.2019.105696.

[16]   J. M. Gagliano and C. E. Frazier, "Improvements in the fracture cleavage testing of adhesively-bonded wood," *Wood and Fiber Science,* pp. 377-385, 2001.

[17]   J. Xavier, M. Oliveira, P. Monteiro, J. J. L. Morais, and M. F. S. F. de Moura, "Direct Evaluation of Cohesive Law in Mode I of Pinus pinaster by Digital Image Correlation," *Experimental Mechanics,* vol. 54, no. 5, pp. 829-840, 2014/06/01 2014, doi: 10.1007/s11340-013-9838-y.

[18]   B. Franke and P. Quenneville, "Analysis of the fracture behavior of Radiata Pine timber and Laminated Veneer Lumber," *Engineering Fracture Mechanics,* vol. 116, pp. 1-12, 2014/01/01/ 2014, doi: https://doi.org/10.1016/j.engfracmech.2013.12.004.